Electrochimica Acta 299 (2019) 626–635

Contents lists available at ScienceDirect

Electrochimica Acta

journal homepage: www.elsevier.com/locate/electacta

Ternary doped polyaniline-metal nanocomposite as high performance supercapacitive material

Anju C.[a], Shiny Palatty [b, *]

[a] Department of Basic Sciences & Humanities, Rajagiri School of Engineering & Technology, Ernakulam, 682039, Kerala, India
[b] Department of Chemistry, Bharata Mata College, Ernakulam, 682021, Kerala, India

ARTICLE INFO

Article history:
Received 12 July 2018
Received in revised form
5 January 2019
Accepted 6 January 2019
Available online 11 January 2019

Keywords:
Conducting polymer
Dielectrics
Energy storage
Capacitance

ABSTRACT

Polyaniline composites incorporating transition metals are still an burgeoning interest as a supercapacitive material due to the formation of metal-PANI hetero junctions. Herein we demonstrate a facile chemical synthesis of ternary doped supercapacitive polyaniline using transition metal as a codopant with an inorganic acid dopant utilizing the oxidant ferric chloride, which itself acts as a dopant. More interestingly the rational combination of external binary dopants can successfully modify PANI morphology. The as synthesized transition metals incorporated PANI (0.7 M Cu^{2+} + 1 M HCl) with a flake like morphology outperform as an energy storage material due to its high surface to volume ratio. Thus the synergistic effect of transitions metals (Cu & Fe) with HCl contribute towards the enhanced electrochemical performance of ternary doped PANI. The frequency dependent dielectric properties, ac conductivity and electrochemical characterizations using cyclic voltammetry and Electrochemical Impedance Spectroscopy of ternary doped PANI has been systematically studied. The ternary doped polyaniline demonstrated a high specific capacitance of 880 F/g and good cyclic stability in 0.1 M H_2SO_4 electrolyte.

1. Introduction

With the growing demand for high efficiency energy-storage devices and technologies the logical world has been actively trying to explore the potentiality of many synergistic blends to bridge the gap between generation and consumption of power. Electrochemical capacitors, batteries and fuel cells are the important storage and conversion devices and among them supercapacitors remain a promising candidate. In comparison to batteries the supercapacitive storage has the uniqueness of fast charge-discharge capability, high energy storage, good cycling stability, high power density and safe operation [1,2]. Supercapacitors are basically classified into Electrical Double Layer capacitors (EDLCs) and Pseudocapacitor based on their mode of charge storage mechanism. The charge storage capability of carbonaceous materials (Graphene, Single wall carbon nanotubes, Multi wall carbon nanotubes etc.) at electrode-electrolyte interface makes it a reasonable contender for electrochemical double layer capacitor (EDLC) applications while the enhanced redox capacity of conducting polymers (Polyaniline, Polypyrrole etc.) and metal oxide (Ni, Fe, In, Co, Ru, Mn etc.) makes it more appropriate for pseudocapacitor applications [3,4]. Synthesis of new hybrid materials with tailored architectures is a necessity to enhance the performance of supercapacitors.

Good environmental stability, ease of synthesis, theoretical high specific capacitance and high conductivity makes polyaniline, the conducting polymer still a burgeoning interest in diverse fields like energy storage, sensors, corrosion protection, electrochromic devices, biomimetic scaffolds, organic light emitting diodes, adsorbents, photovoltaic cells etc [5–12]. Also the active –NH group in PANI chain has enjoyed a revival of scientific interest which makes it a good candidate in energy storage and conversion devices. The myriad of chemical structures shown by PANI like fully oxidized pernigraniline form, half oxidized emeraldine base and fully reduced leucoemeraldine form has made its redox chemistry a complicated one. Apart from the above three forms some other intermediate redox states like protoemeraldine and nigraniline are also defined [13]. Due to the transition between various oxidation states PANI acts as an active material in storing charges via redox reactions but low practical capacitance and poor cycle stability due to its structural detoriation during repetitive charge-discharge

* Corresponding author.
E-mail addresses: anju.chonat@gmail.com (C. Anju), shinypalaty@gmail.com (S. Palatty).

https://doi.org/10.1016/j.electacta.2019.01.030
0013-4686/

cycle and over oxidation at higher potentials limits the use of PANI in capacitors [14–16]. Such intrinsic defects of PANI can be surpassed by developing polymer–inorganic architectures. The presence of Zn^{2+}, Ti^{4+}, Cu^{2+} and Fe^{3+} can effectively enhance the energy density of PANI matrix while stabilizing the polymer for longevity by taking part in redox process [17]. A coadjutant effect beneficial for PANI matrix is exhibited by such designs by retaining the original intrinsic performances.

The backbone of PANI comprises of two groups-electron rich benzenoid group (amine nitrogen) and electron deficient quinoid group (imine nitrogen) which possess different activity. The transition from insulator to metallic phase supported by proton-induced conversion without changing the number of electrons makes PANI an efficient candidate among conducting polymers [18]. Dopants can communicate specifically with the polymer chain by means of oxidative doping at amine nitrogen, protonation of imine nitrogen by protonic acids, Lewis acids or by pseudoprotonation by alkali metal ions. Apart from essential dopants there are substances which can generously upgrade the conductivity of PANI which additionally expands the concept of doping to secondary doping, solvation, counter ion-induced processibilty and molecular recognition [19]. An association stronger than Vander Waals forces through the incorporation of transition metal into the PANI matrix by coordination via nitrogen atoms creates metal-PANI hetero junctions which play a critical role in many energy harvesting applications [20]. The synthesis of conductive PANI by using transition metal salts was first reported by Dimitriev [21]. Polyaniline containing transition metal ions was investigated by Yang et al. [22]. Conformational changes happening in the polymer backbone is crucial to tweak many novel physical and chemical properties and the mechanism of doping depends on the kind of transition metal utilized.

The nature of oxidant especially its redox potential has a solid impact in controlling the morphology and properties of PANI. Persulphates (APS) are the commonly used oxidising agent in the oxidative polymerisation of aniline. The polymerisation proceeds at a lower rate with $FeCl_3$ since its redox potential (0.77 V) is lower than persulphate (2.0 V) [23]. But the real disadvantage with APS is that it is stochiometrically devoured in the reaction which generates acidic byproducts [24]. Secondary reactions are not much observed when persulphates are supplanted by $FeCl_3$ which itself can act as an oxidising agent as well as a codopant [23]. Also active spots can undergo autocatalytic polymerisation by using HCl generated from the polymerisation using $FeCl_3$ [25]. An environmental friendly synthesis of PANI with $FeCl_3$ as catalyst and ozone as oxidant and its reaction kinetics was investigated by Toshima et al. where the only by product formed during the reaction is water [26]. Kinetics of $FeCl_3$ initiated aniline polymerisation was studied by Gordana et al. [24]. A one pot synthesis of polyaniline using $FeCl_3$ as oxidising agent as well as a codopant was done by Alessandro et al. to bridge electrochemical and electronic devices [23].

Not much work was reported on the combined effect of transition metal dopant with an inorganic acid dopant in the synthesis of PANI for energy storage applications. Li et al. reported the preparation of PANI by using codopants Zn^{2+} and H^+ and investigated its performance as supercapacitors [27]. Debasis Ghosh et al. studied H^+ and Ni^{2+} codoped Polyaniline-MWCNTs composite for supercapacitor applications [28]. In this contribution we detailed the effect of transition metal (Cu^{2+}) as a codopant with HCl dopant on the supercapacitive performance of PANI synthesized using $FeCl_3$ as oxidising agent (which also act as a dopant) by in situ chemical oxidative polymerisation method. Since the sort of dopant has a profound influence in tuning the performance of PANI, the examination of the response utilizing binary and ternary dopants was likewise done. The capacitive performance of as prepared PANI was contemplated by using Dielectric, Cyclic Voltammetry (CV) and Electrochemical Impedance Spectroscopy (EIS) studies. Additionally morphological, structural and electrical properties were also studied.

2. Experimental sections

2.1. Materials

Aniline was double distilled prior to use. Anhydrous Ferric chloride ($FeCl_3$), Copper sulphate ($CuSO_4.5H_2O$), Hydrochloric acid (HCl) and acetone were of analytical grade and were used without any treatment.

2.1.1. Synthesis of ternary doped PANI- metal nanocomposite

Polyaniline-metal nanocomposite was prepared by rapid mixing polymerisation method by using HCl and $CuSO_4.5H_2O$ as external binary dopants and anhydrous $FeCl_3$ as oxidant (also act as a dopant). To prepare PANI different concentrations of $CuSO_4.5H_2O$ (0.3 M, 0.5 M, 0.7 M and 1 M) was added to 0.1 M aniline and the solution was stirred for half an hour. The oxidant 0.3 M $FeCl_3$ solution made in 1 M HCl was rapidly added to the aniline-copper solution. The reaction was kept overnight without any agitation. The resultant dark green precipitate was filtered with vacuum pump and then washed with distilled water and acetone until the filtrate become colourless. Finally it was dried in an oven at 80 °C for 24 h.

2.1.2. Synthesis of binary doped PANI- metal nanocomposite

To compare the effect of ternary doped PANI, binary doped PANI composite was also synthesized by using single external dopant with anhydrous $FeCl_3$ as oxidant (also act as a dopant). To prepare PANI with HCl dopant 0.3 M $FeCl_3$ solution made in 1 M HCl was rapidly added to 0.1 M aniline solution. Synthesis of PANI using $CuSO_4.5H_2O$ as external dopant was done by adding 0.3 M $FeCl_3$ solution to aniline (0.1 M) - $CuSO_4.5H_2O$ (0.7 M) solution (which was initially stirred for half an hour). The reaction was kept overnight without any agitation. The resultant dark green precipitate was filtered with vacuum pump and then washed with distilled water and acetone until the filtrate become colourless. Finally it was dried in an oven at 80 °C for 24 h.

2.2. Material characterization

The investigation of structural composition of PANI samples was done by using Fourier Transform Infrared spectroscopy (Thermo Nicolet, Avatar 370), UV–Visible spectroscopy (Varian, Cary 5000) and X-ray Diffraction analysis (Bruker AXS D8 Advance). Morphological characterisation was studied by using scanning electron microscope (TESCAN VEGA 3 SBH), SEM-EDS (OXFORD XMX N) and High resolution Transmission Electron Microscope (Jeol/JEM 2100). Dielectric performance and ac conductivity measurements were evaluated by using an Agilent LCR series meter- E4980 A from 100 Hz to 2 MHz on compressed PANI pellets at room temperature. The electrochemical characterizations of ternary doped PANI were done by using Cyclic Voltammetry (CV) and Electrochemical Impedance Spectroscopy (EIS). EG&G potentiostat (model 263 A) which is interfaced to a PC through a GPIBcard (National instruments) was used for Cyclic Voltammetry studies. Electrochemical Impedance Spectroscopy studies was done by using a model 5210 lock-in amplifier (Perkin-Elmer instruments) with Powersuite software (EG&G) interfaced with a PC in a frequency range of 100 MHz to 100 KHz. CV and EIS experiments were done by using a working electrode (graphite electrode), counter electrode (Platinum foil) and a reference electrode (Ag/AgCl/3 M NaCl) with

0.1 M H_2SO_4 as the supporting electrolyte. The sample was first dispersed in DMF and the dispersion was dropped onto a graphite electrode to form a film which was allowed to dry at room temperature.

3. Results and discussions

3.1. Morphology

The practical properties and applications of a macroscopic material depends on its final morphology where PANIs propensity towards various morphologies are influenced by rate and type of nucleation (homogeneous or heterogeneous), growth of the ultimate products in solid-state reaction, concentration of aniline and type and amount of dopants and oxidizer in the reaction medium. Also the type of counter ion plays a critical role in moulding PANIs morphology. After doping PANI with transition metal salts a significant change in the conformation of PANI is mentioned in the literature [20].

SEM and TEM analysis were carried out for the morphological study of ternary and binary doped PANI and was depicted in Figs. 1 and 2. SEM image of binary doped PANI synthesized by using 0.7 M Cu^{2+} shows highly entangled morphology with no vacant sites. This could be due to the coordination geometry of transition metal cation i.e. copper with its coordination number less than or equal to six can provide inter and intra chain connections among PANI chains [3] (Fig. 3) and the TEM images confirmed the presence of interconnected bead like morphology (Fig. 2c, d) (more TEM images shown in SI-1) to form an entangled chain arrangement. Such bead like conformation arises due to the non availability of sufficient H^+ ions in the medium to form polyanilinium salts [29]. But the PANI sample prepared by using HCl as external dopant has a branched fibrous morphology [30] (supported by TEM-Fig. 2e). SEM-EDS analysis of $FeCl_3$–HCl system (Fig. 4a) substantiates the ability of $FeCl_3$ to act as both oxidising agent and a codopant and that of $FeCl_3$–Cu^{2+}–HCl (Fig. 4b) confirmed the presence of both Fe and Cu in the PANI matrix which further demonstrates various stochiometric compositions maintained in the sample (SI-2).

In the case of ternary doped PANI with the increase in concentration of Cu^{2+}, entangling of PANI chains increases and also some mixed surface morphologies were observed (Fig. 1a, b, c, 1d). At 0.7 M Cu^{2+} concentration some flake like structures are seen along with agglomerated PANI chains which explain the importance of the correct stochiometric proportion of external binary dopants in tuning PANI morphology for different applications. Also the presence of phenazine like structures (supported by FT-IR) supports the formation of such flake like morphology. Phenazine units are formed by the oxidation of ortho coupled aniline units which are formed by the initial oxidation of neutral aniline molecules [31]. Due to low solubility and flat structure phenazine units precipitate as plate like crystallite and can act as a template for further growth of PANI [32]. Flake like morphology of ternary doped (0.7 M Cu^{2+} + 1 M HCl) PANI is confirmed by TEM analysis (Fig. 2a, b) (more TEM images shown in SI-1) which by its nature could effectively hold metal particles on its surface compared to entangled fiber like or bead like morphologies and hence play a significant role in enhancing energy storage applications.

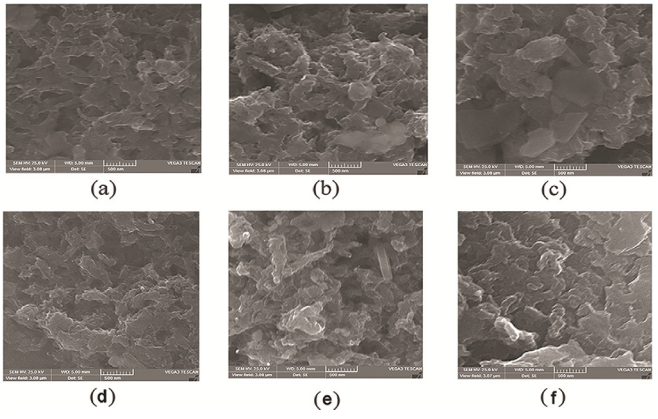

Fig. 1. SEM image of ternary doped PANI with a) (0.3 M Cu^{2+} + 1 M HCl) b) (0.5 M Cu^{2+} + 1 M HCl) c) (0.7 M Cu^{2+} + 1 M HCl) d) (1 M Cu^{2+} + 1 M HCl) and binary doped PANI with e) 1 M HCl f) 0.7 M Cu^{2+}.

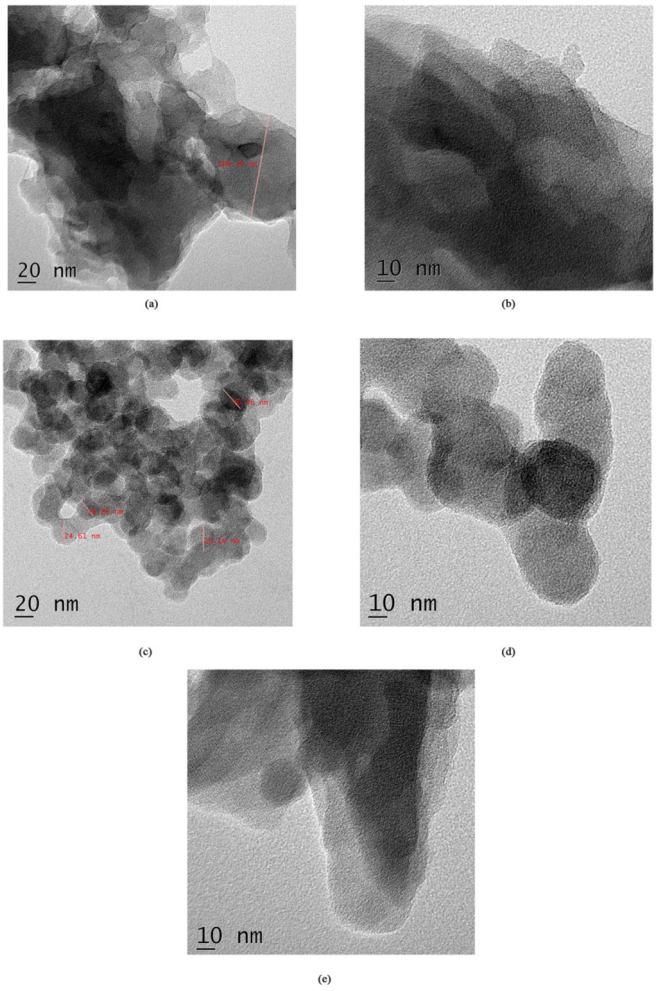

Fig. 2. TEM image of ternary doped PANI with a) (0.7 M Cu^{2+} + 1 M HCl) at 20 nm b) (0.7 M Cu^{2+} + 1 M HCl) at 10 nm and binary doped PANI with c) 0.7 M Cu^{2+} at 20 nm d) 0.7 M Cu^{2+} at 10 nm e) 1 M HCl at 10 nm.

3.2. Chemical structure

3.2.1. FT-IR

The molecular structural changes happened in the PANI matrix by the introduction of ternary and binary dopants were characterized by FT-IR spectroscopy. The FT-IR spectrum of H^+ doped PANI, Cu^{2+} doped PANI and H^+ and Cu^{2+} co-doped PANI at different concentrations with ferric chloride oxidant were depicted in Fig. 5. The above spectra of PANI prove the formation of conducting emeraldine salt form. The origin of absorption band around 3200-3400 cm^{-1} corresponds to N–H stretching vibration. The

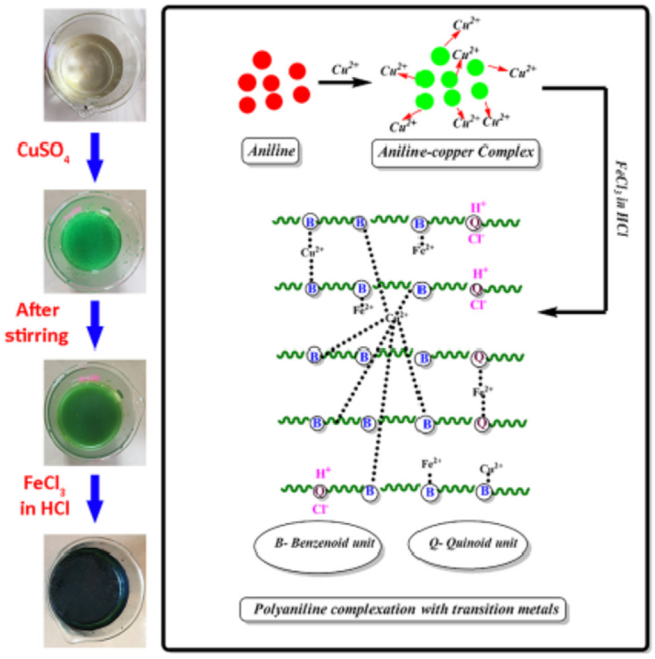

Fig. 3. Schematic representation of transition metals complexation with PANI.

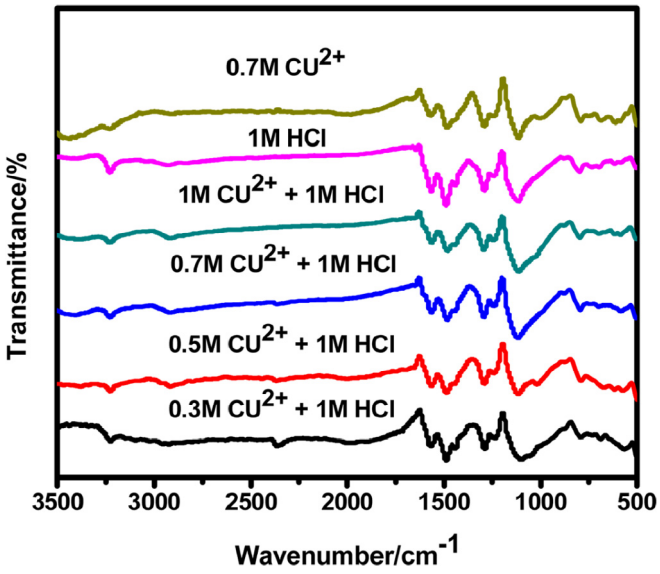

Fig. 5. FT-IR spectra of ternary and binary doped PANI at different concentrations.

appearance of the peak around 2925-2917 cm^{-1} reflects the stretching vibrations of SP^2 hybridized C–H bonds. The peaks centred around 1565-1570 cm^{-1}, 1481-1492 cm^{-1} represents C=C stretching vibration of quinoid diimine rings (>C=N-) and benzenoid diamine moieties and the FT-IR peaks concentrated around 1289-1293 cm^{-1} and 1237-1242 cm^{-1} indicates C–N stretching of quinoid and bezenoid units. The peaks around 1096-1114 cm^{-1} represents C–N stretching vibrations in $B–NH^{+}=Q$ (B-benzenoid, Q-quinoid) and is an indication of protonated form of conducting PANI. Out of plane C–H bending vibrations results in many low intensity peaks between 791 and 797 cm^{-1} and is the evidence for the formation of 1,4 substituted phenylene rings.

Cu^{2+} ternary and binary doped PANI shows broad peaks than HCl doped PANI due to the interaction of transition metal cations with the lone pairs of nitrogen atom of benzenoid and quinoid moieties in PANI host matrix [33]. The blue shift in the position of peak with the peak broadening indicates higher degree of charge delocalization by proton induced spin unpairing mechanism with the formation of radical cation or semiquinone group [28]. The peak corresponding to protonated PANI is partitioned into two at 1112 cm^{-1} and a shoulder at 999 cm^{-1} pointing to the fact that imine nitrogen experiences pseudoprotonation with Cu^{2+} dopant [34]. On comparing with Cu^{2+} binary doped PANI the peak around 1112 cm^{-1} in ternary doped state is more sharp and intense which substantiate improved doping levels. The band due to para disubstituted aromatic rings still exists in ternary dopant combination with some shift in its peak positions confirming the interaction of PANI with metal cations. All these changes indicate the synergistic effect of transition metal cations (Cu & Fe) with HCl dopant on PANI. For ternary doped PANI a sharp intense band of protonated PANI is seen at 0.7 M Cu^{2+} concentration and this might be due to the presence of more number of phenazine units since the presence of phenazine units can be identified by the appearance of peak around 1108 cm^{-1} [35].

3.2.2. UV–visible spectroscopy

The UV– Visible spectrum of ternary doped PANI at different concentrations is depicted in Fig. 6. The above spectra of PANI show three transitions at 340, 370 and 600 nm. The sharp intense peak around 340 nm can be assigned to pi-pi* transition of benzenoid ring which is a HOMO- LUMO electronic transition and also ascribed to the excitation of benzenoid units of PANI chain. The prominent shoulder at 370 nm corresponds to the characteristics

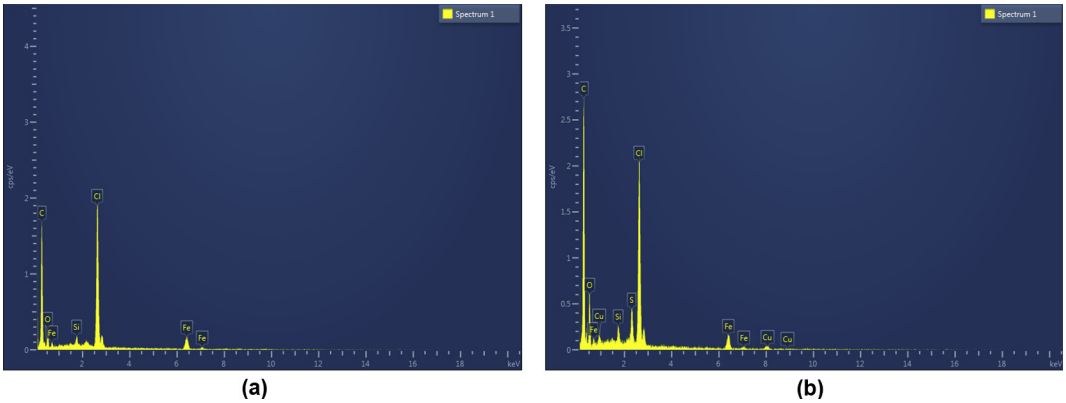

Fig. 4. SEM-EDS analysis of a) Binary doped PANI with 1 M HCl b) Ternary doped PANI with (0.7 M Cu^{2+} + 1 M HCl).

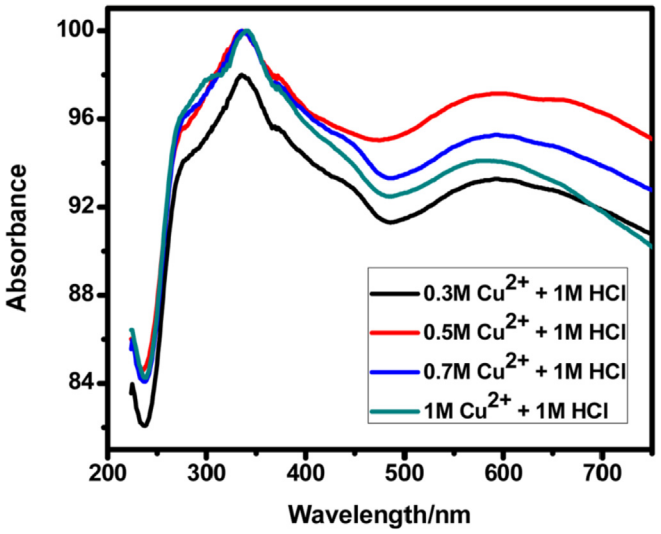

Fig. 6. UV– Visible spectra of ternary doped PANI at different concentrations.

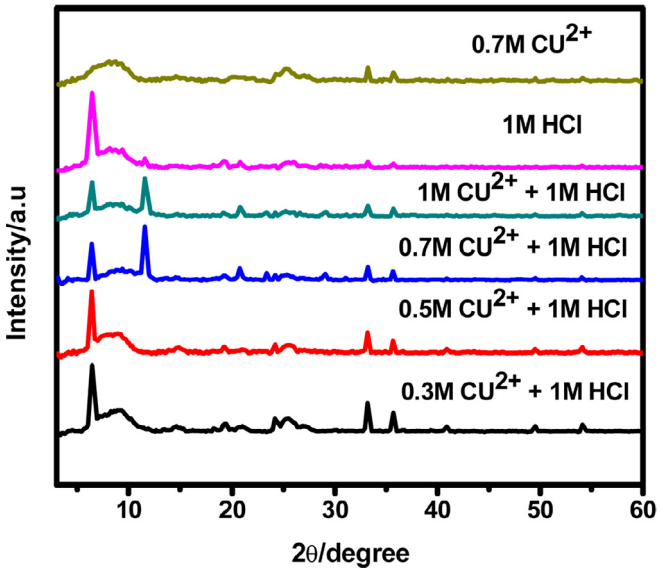

Fig. 7. XRD pattern of ternary and binary doped PANI at different concentrations.

peak of protonated polyaniline from polaron-pi* transition. The long tail at 600 nm relates the transition of benzenoid unit into quinoid moiety i.e. n-pi* electronic transition. This peak confirms the as synthesized polyaniline in its emeraldine salt form. For ternary doped PANI with the increase in concentration of Cu^{2+} from 0.5 M to 1 M the quinoid absorption band diminishes with some blue shift due to the enhanced interaction of transition metal cations with imine nitrogen. In fact the benzenoid pi-pi* transition peak remains almost identical with some peak broadening. But at lower concentration of Cu^{2+} (0.3 M) the absorption of the peaks corresponding to both pi-pi* transition of benzenoid ring and n-pi* transition of quinoid moiety is highly reduced and this might be due to the coordination of more number of metal nanoparticles with amine and imine nitrogen of PANI (supported by XRD).

3.3. Crystallinity

The crystalline nature of the samples was investigated using XRD analysis. The XRD pattern of PANI prepared by using ternary and binary dopants are shown in Fig. 7 and it shows the characteristic peaks of emerladine salt form of PANI at 2theta values around 20 and 25. The above peaks indicate (020) and (200) crystalline planes of PANI and it correspond to periodicity parallel and perpendicular to the conjugation chains of PANI. Also the peak corresponding to (022) plane is seen around 2theta value of 29 and some lower diffraction peaks appeared around 6 and 12. The effective penetration of dopants results in peaks at lower 2theta values and these kinds of peaks are only seen in highly ordered samples [36]. Khalid et al. claimed that the periodic distance between the dopant and the N atom on adjacent chains results in a peak around 6.5 [37]. This peak corresponds to the interdigitations and crystallization of side chain PANI resulting in a lamella formation between polyaniline chains. The type of dopant and the doping level has a profound influence in the intensity of such lower diffraction peaks. Also the peak around 2theta 41 is an indication of long range high orientation of PANI chain [29]. Apart from the above mentioned peaks some additional peaks are seen around 2 theta values 33, 36, 49 and 54 which might be due to the formation of copper oxide nanoparticles in PANI matrix representing (110), (002), (202) and (020) planes [38].

On comparing with H^+ doped PANI the peaks of Cu^{2+} binary doped are more broadened indicating an amorphous nature due to the incorporation of Cu^{2+}. Most of the peaks of ternary doped PANI manifest more crystallinity than binary doped one due to the combined effect of HCl with transition metal cations indicating that the ternary doped condition supports PANI crystallization by forming more number of nucleation sites. With the increase in concentration of Cu^{2+} the lower diffraction peaks and the peaks corresponding to conducting PANI becomes thinner and prominent which implies a better crystallinity of PANI by a more ordered interchain stacking in between PANI chains. Above 0.7 M concentration of Cu^{2+} the lower diffraction peaks starts broadening indicating the deviation to amorphous nature. Also SEM and TEM images reveal that PANI synthesized using external binary dopants 1 M HCl with 0.7 M Cu^{2+} has some flaky morphology and XRD peak pattern confirms that the flake like PANI has the highest crystallinity. Thus it is concluded that the although the presence of HCl dopant with $FeCl_3$ can provide some amount of crystallinity to PANI samples the addition of accurate stochiometric proportion of Cu^{2+} to $FeCl_3$–HCl system can enhance the crystalline character with highly ordered stacking of PANI chains.

3.4. Dielectric studies

A study on dielectric response and ac conductivity measurements can provide an idea about charge transport mechanism in polyaniline. At room temperature a high dielectric constant is essential for a material in order to utilize its potentiality in assorted applications. As far as electronic industry is concerned understanding the nature of dielectric with varying frequency is desirable. Polyaniline is a promising dielectric material and the polarizability of the constituents supported by atomic, interfacial, electronic polarizations and dipoles contribute to its dielectric properties. Dielectric studies were done in a frequency range of 100 Hz-2 MHz on PANI pellets sandwitched in between the plates of LCR meter in order to frame a parallel plate capacitor at room temperature.

3.4.1. Dielectric constant

Dielectric constant which is an important electrical property is the ability of the material to get polarized and to store charges under the influence of an electric field. The development of a permanent “dipole moment” due to the structural charge density

differences over intramolecular distances and the "polarizability" or the induced change in dipole moment due to the changes in the molecular electronic distribution by an electric field are the two molecular properties over which the dielectric constant shows a strong dependency [39].

Frequency assisted dielectric constant ε' at room temperature are represented in Fig. 8.a over a frequency range from 100 Hz to 2 MHz The capacitance of the pellet and its geometry contribute towards the dielectric constant of PANI. Dielectric constant can be evaluated from the measured capacitance (C), thickness (d) and area of the pellet (A) by using the relationship $\varepsilon' = C\ d/\varepsilon^0 A$ where ε^0 is the dielectric permittivity in vacuum (8.85×10^{-12} Fm^{-1}). In order to substantiate the role of dopants in improving the dielectric properties of PANI a comparison between ternary and binary dopants are demonstrated in the figure. For all the samples dielectric constant is high at lower frequencies with a sharpest decrease with frequency due to the accumulation of charge carriers at the internal interfaces known as Maxwell-Wagnar-Sillars effect and thereafter it remains constant at higher frequencies due to the inability of induced dipoles to allign with the variation in frequency of the applied field known as dielectric relaxation phenomenon [40].

From the figure it is clear that at a particular frequency the dielectric constant of most of the PANI samples synthesized using Cu^{2+} metal dopant are higher than those synthesized with HCl dopant signifying the role of transition metals in enhancing storage performance of PANI. The presence of Cu^{2+} in PANI matrix makes it an ideal capacitive system since the PANI degradation can be reduced by adhesion strength of PANI chain obtained due to the multiple doping sites of Cu^{2+} ion [41]. These manifold sites can coordinate adjacent PANI chains by forming interchain linkages. These sorts of organic-inorganic association are advantageous for supercapacitors. Also the presence of Cl^- in PANI matrix can enhance interfacial polarization [42].

For ternary doped PANI the dielectric constant value increases with increase in concentration of Cu^{2+} from 0.5 to 0.7 M and thereafter it decreases. The availability of active sites are improved by the intermolecular interaction of PANI with external binary dopants Cu^{2+} and H^+ which finally helps to improve its charge storage capacity [17]. With the increase in concentration of Cu^{2+} more number of metal ions will come closer to form bipolaron structure thus increasing dielectric constant [43]. At higher concentration entangling of PANI chain can block the conductive pathway and thus decreases the capacitive performance. The improved dielectric constant observed at lower concentration of Cu^{2+} may be due to the interaction of more number of metal nanoparticles with PANI chain (supported by XRD). Morphology is an important factor on which the dielectric properties depend. The improved dielectric performance of HCl doped PANI can be assigned to its branched fibrous structure. The highest dielectric constant observed for 0.7 M Cu^{2+} ternary doped PANI can be explained by its flake like morphology. Flake structures has the advantage of large surface to volume ratio when compared to fibrous or spherical ones which makes better interaction with dopants thereby promoting good delocalization and improves the storage capacity [44].

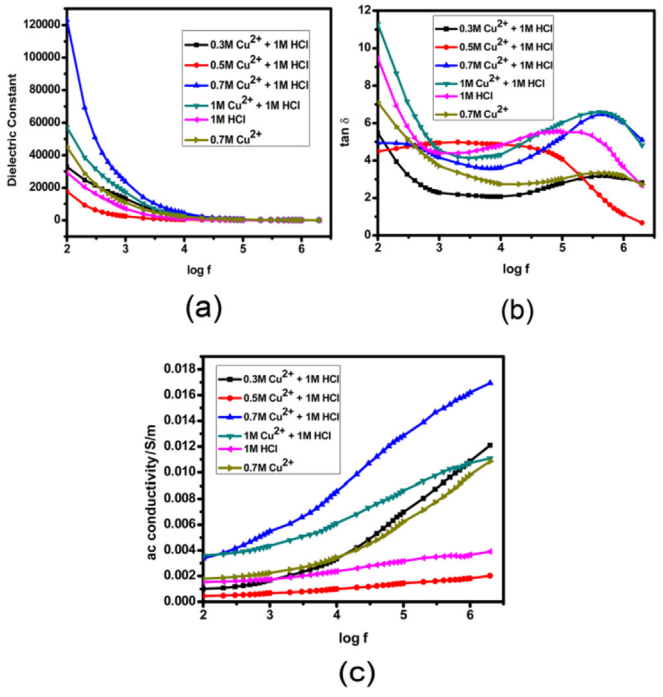

Fig. 8. Frequency dependence of a) Dielectric constant b) Tangent loss c) ac conductivity of ternary and binary doped PANI.

3.4.2. Tangent loss

Fig. 8.b shows tangent loss as a function of frequency. Tangent loss is related to the power of dielectric loss of the material [8] and is calculated using the equation $\tan\delta = \varepsilon''/\varepsilon'$ where $\varepsilon'$is the dielectric constant and ε'' is the dielectric loss. The loss values of all the PANI samples shows similar behaviour as that of dielectric constant with a higher loss values at lower frequencies which then decrease abruptly with the increase in frequency and at higher frequencies it remains almost constant. A doped PANI system comprises of mobile polaron-bipolaron system and the dipoles with restricted mobility. Mobile charges within the polymer matrix causes a high dielectric loss values at lower frequencies [45]. The contribution of interfacial polarization decreases with increase in frequency since the masses involved for interfacial polarization are greater than the average dipoles [46]. At higher frequency region insufficient ion diffusion in the direction of electric field due to the fast periodic field reversal decreases charge accumulation resulting in a low loss factor [45]. Fig. 8.b shows that the tangent loss values observed for most of the ternary doped PANI except at higher concentration is less compared to that of binary doped ones at lower frequency side which further supports the significance of ternary dopants in PANI matrix in enhancing electrochemical storage capacity. At higher concentrations of Cu^{2+} i.e. 1 M Cu^{2+} in ternary doped and 0.7 M Cu^{2+} in binary doped PANI the free movement of H^+ ions along the polymer chain is inhibited by Cu^{2+} accumulation resulting in a large interfacial polarization. Thus a free charge motion differences results in a high tan δ value at higher concentrations of Cu^{2+} [47].

3.4.3. AC conductivity

Since conducting polymers are not having any permanent dipoles there exists a random charge trapping of Quasi-particles like solitons, polarons and bipolarons which are produced from a lattice distortion and they are responsible for the charge transport in conducting polymers. Short range ac conductivity and long range dc conductivity arises from charge hopping between the nearest redox sites on the polymer chain due to electric field relaxation. Interfacial polarisation and inhomogeneous system in the PANI matrix are responsible for the frequency depended behaviour of ac conductivity in conducting polymers [45].

The fluctuations of ac conductivity with increasing frequency are shown in Fig. 8.c. The ac conductivity σ(ac) was calculated from $\sigma ac = 2\Pi f\varepsilon''\varepsilon^0$, where σ(ac) is the ac electrical conductivity (S/cm); f is the applied frequency (Hz); ε" is the dielectric loss. The ac

conductivity of all the samples increases with increase in applied frequency due to the formation of large number of quasi particles. The conductivity of most of the PANI samples synthesized using Cu^{2+} metal dopant is higher than HCl dopant. Due to the accumulation of mobile charges at the interfaces and dipole formation on the metal complex, interface charge polarization (the Maxwell–Wagner–Sillars effect) and intrinsic electric dipole polarization are more prominent in a heterogeneous metal polymer system [46]. When transition metal is added to polyaniline matrix the lone pairs of nitrogen gets easily coordinated with the d orbital of transition metal which can provide an easy conductive pathway. So during the complexation process the donor nitrogen remains as an electron deficient centre which increases the conductivity [48]. This kind of interaction will occur not only at the surface but also throughout the bulk material as a result the number of charge carriers per unit volume is enhanced which causes an augmentation in the conductivity of PANI. Also the bonding with the dopant can create various conductive path of different length in the PANI chain through an enhanced coordination between polymer chain pi electron density and transition metal. The complexation process can create some additional energy levels in between HOMO-LUMO energy gap thereby decreasing the band gap [49].

Of all the prepared samples the highest conductivity is observed with 0.7 M Cu^{2+} ternary doped PANI. With the increase in concentration of Cu^{2+} charge carriers are easily transported by strong hopping through the defect sites along the polymer chain in ternary doped PANI. But at higher concentrations due to the formation of metal clusters at the interface conductivity and polarization are inhibited [45]. Thus the decrease in conductivity after 0.7 M Cu^{2+} may be due to the strong agglomeration of PANI matrix which blocks the conductive path and reduces the conjugation length. Also structural modifications happened in the PANI morphology has a remarkable effect in electronic distributions thereby reflecting in the conductivity values and this may be the reason for higher conductivity of (0.3 M Cu^{2+} + 1 M HCl) doped PANI than (0.5 M Cu^{2+} + 1 M HCl) doped one. SEM image of (0.3 M Cu^{2+} + 1 M HCl) doped PANI shows fibre like morphology with some expanded coil conformation which leads to the formation of more number of metal nano particles (supported by XRD). Such expanded conformation results in a polaron band with a wide dispersion in energy due to an efficient interaction between adjacent PANI chains [37]. The highest conductivity of 0.7 M Cu^{2+} ternary doped PANI also rely upon its flake like morphology which is highly crystalline (supported by XRD). Crystallinity and conductivity of conducting polymers are strongly correlated thereby increasing the bulk conductivity.

3.5. Electrochemical studies

3.5.1. Cyclic voltammetry

The capacitive performance of 0.7 M Cu^{2+} ternary doped polyaniline was confirmed by cyclic voltammetry tests. Fig. 9.a Illustrates CV curve of ternary doped PANI and bare graphite at a scan rate of 50 mV/S and Fig. 9.b at different scan rates 10, 20, 50, 100, 200 and 500 mV/s measured in a voltage window of −0.1 V to 0.6 V. An ideal capacitive behaviour is indicated by the formation of a quasi rectangular shape of CV plot with large current and symmetry in anodic and cathodic direction. The negative and positive current in CV curve is the result of cathodic reduction and anodic oxidation. The characteristic peaks seen in the CV curve are the evidence for pseudo capacitive behaviour of the material [50]. The faradaic transformation of emeraldine-pernigraniline form of PANI results in a pair of redox peaks during charge discharge process [51,52].

Specific capacitance is calculated from Cyclic Voltammogram studies using the equation

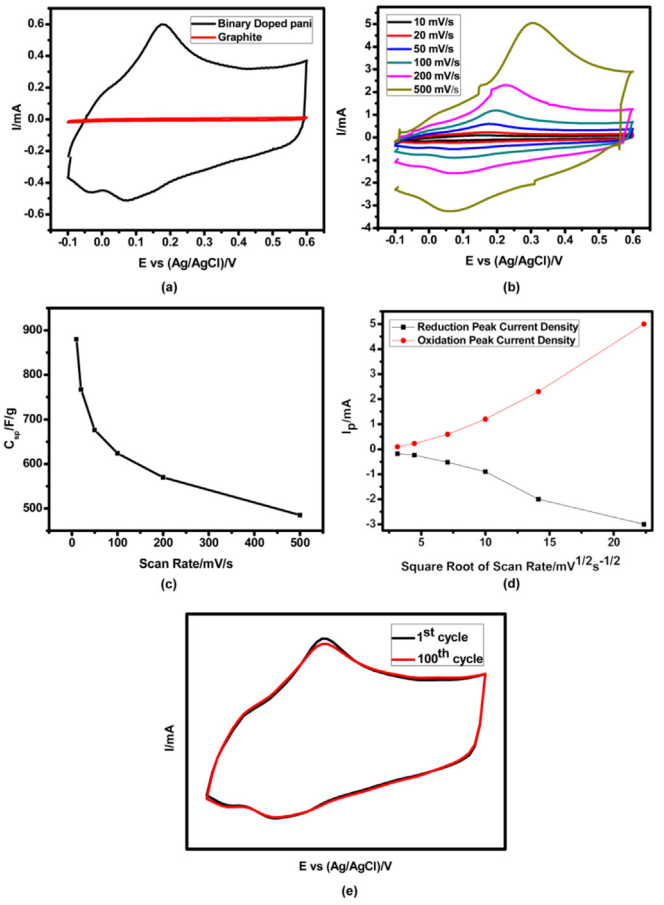

Fig. 9. a) CV voltammogram of (0.7 M Cu^{2+} + 1 M HCl) ternary doped PANI and bare graphite at a scan rate 50 mV/s b) CV voltammogram of (0.7 M Cu^{2+} + 1 M HCl) ternary doped PANI at different scan rate c) Specific capacitance of (0.7 M Cu^{2+} + 1 M HCl) ternary doped PANI at different scan rate d) Plot of oxidation and reduction peak current Vs square root of scan rate of (0.7 M Cu^{2+} + 1 M HCl) ternary doped PANI e) CV voltammogram of (0.7 M Cu^{2+} + 1 M HCl) ternary doped PANI at a scan rate of 200 mV/s after 100 cycles.

$$C_{sp} = \frac{\int_{v_1}^{v_2} i(v)dv}{2(v_2 - v_1)\, m\, s}$$

where numerator denotes the total charge under CV curve, $(v_2 - v_1)$ is the potential window, m is the mass of the electrode and s is the scan rate [48]. The specific capacitance value at different scan rates 10, 20, 50, 100, 200 and 500 mV/s are shown in Fig. 9c and is found to be 880, 767, 676, 624, 570 and 485 F/g. The number of active sites at the electrode, mobility of ionic species and the ease of insertion −desertion of electrolyte ions in the polymer matrix are the factors on which the Faradaic current at electrode − electrolyte interface depends [3]. The synergistic effect of ternary dopants contributes towards high capacitance supported by decrease of internal resistance and increase in electrolyte ion transport rate due to good conductivity. The combined contribution of flake like morphology with good charge delocalization due to the presence of transition metal cations in polymer matrix facilitates appreciable fast ionic transport which further plays a key role in enhancing the capacitive performance of 0.7 M Cu^{2+} with 1 M HCl codoped PANI. Additionally the presence of positive ions (H^+ and transition metal cations) could contribute towards pseudo faradaic reaction [3].

With the increment in scan rate from 10 to 500 mV/s specific

capacitance value decreases from 880 to 485 F/g. The above behaviour may be due to the inability of inner active sites to precede the redox transitions completely [50,53]. The region in which the current directions are abruptly inversed i.e. transient region and interfacial capacitance region can be affected by the change of sweep rate[3]. The kinetic effects and uncompensated ohmic drop results in predominant shifts of oxidation and reduction peaks with improved current density i.e. with the increase in scan rate the peak potential shifts to higher positive and negative side during reduction and oxidation process [50]. At higher sweep rate slower pseudo capacitive redox reaction, large electrochemical polarization and higher diffusion resistance faced by the electrolytic species to travel in the PANI host matrix causes a decrement in the capacitive performance [51,54]. The increased resistance is attributed to the decrease in doping dedoping mechanism of PANI due to the inadequate time for ionic transport at higher scan rate [55]. But the retention of redox peaks at higher scan rate confirms good electrochemical capacitive performance and good rate capability of as synthesized PANI material.

Fig. 9.d represents the peak current of ternary doped PANI Vs square root of scan rate which shows a direct proportionality between current and scan rate indicating diffusion controlled electrochemical process signifying an efficient capacitive nature [56]. The total current observed in the CV response of polyaniline is the combination of faradaic and capacitive contribution where the amount of oxidized polymer controls the capacitive contribution [57]. The stability of the electrode was further examined by cycle life tests where 100 cycles are run on the material at a scan rate of 200 mV/s shown by Fig. 9.e where the CV curve still maintains the pseudo rectangular shape. The CV curve obtained in the first cycle and 100th cycle is almost similar indicating a very good retention of capacitive performance even after 100 cycles. Good cycle stability of ternary doped PANI can be attributed to the improved intermolecular and pi-pi interaction of transition metal cation with PANI host matrix which could further resist the change in conductive pathway during charge-discharge process [54].

3.5.2. Electrochemical Impedance Spectroscopy

In order to further evaluate the supercapacitive performance of ternary doped PANI Electrochemical Impedance Spectroscopy measurements was done in a frequency range of 100 MHz to 100 kHz at AC amplitude of 10 mV at open circuit potential (Fig. 10). To fit the experimental data an equivalent circuit is also proposed from EIS studies. The complex phenomena of electron interception and diffusion at electrode-electrolyte interface can be studied by Electrochemical Impedance Spectroscopy (EIS) which is a frequency domain technique, which further throws an insight into the influence of doping and redox additive electrolyte on the resistive and capacitive element of supercapacitor [3]. Generally high frequency region reflects the electrolyte properties and the middle frequency area assigns to the electrode-electrolyte interface properties [58]. The sudden increment in the Z_{im} value with almost a vertical line at lower frequency portion of Nyquist plot is ascribed to the capacitive behaviour of ternary doped PANI. The resistance of the charge transfer over the interface between the electrode and electrolyte is reflected by the charge transfer resistance value (R_{ct}) [59,60]. The above Nyquist plot of ternary doped PANI showed a drastic decrease in R_{ct} value (shown in SI-4) which can facilitates the charge transfer process [61] i.e. an easier intercalation and deintercalation of charges. The lower R_{ct} value may be due to the effective interaction between PANI and transition metal cations, the high surface to volume ratio attained from 2-D flake like morphology and good crystallinity which helps PANI for an efficient diffusion of charges and finally contribute towards an appreciable supercapacitive behaviour.

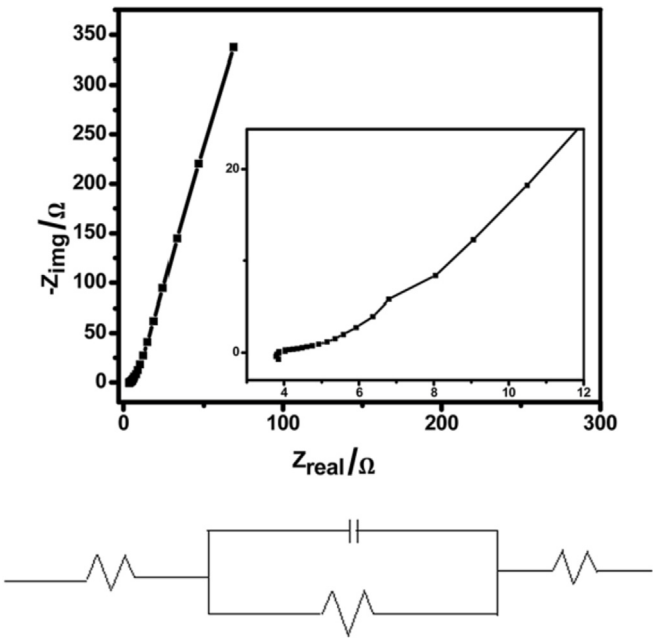

Fig. 10. Nyquist plot of (0.7 M Cu^{2+} + 1 M HCl) ternary doped PANI in a frequency range from 100 MHz to 100 KHz with an equivalent circuit fitting.

4. Conclusions

In summary, we have demonstrated an enhancement in the electrochemical performance of ternary doped PANI synthesized using varying concentration of Cu^{2+} (0.3, 0.5, 0.7 & 1 M) with 1 M HCl and 0.3 M $FeCl_3$ oxidant. Dielectric studies reveal a high dielectric constant for PANI synthesized using external binary dopants 0.7 M Cu^{2+} and 1 M HCl. Further electrochemical investigations done by using Cyclic Voltammetry and EIS studies affirmed the potentiality of ternary doped PANI to act as an efficient supercapacitive material. Ternary doped PANI exhibits a high specific capacitance of 880 F/g at a scan rate of 10 mV/s and good cycle stability in 0.1 M H_2SO_4 electrolyte. The Nyquist spectra obtained from EIS studies has a very small charge transfer resistance value suggesting an easier intercalation and deintercalation of charges. The improved electrochemical behaviour of ternary doped PANI is also attributed to its morphology. SEM and TEM images uncover the role of correct stochiometric proportion of Cu^{2+} and H^+ in tuning PANI morphology. Flake like PANI obtained at external binary dopant combination of 0.7 M Cu^{2+} and 1 M HCl has the advantage of large surface to volume proportion when compared to fibrous or spherical ones which enhances the interaction with dopants thereby advancing great delocalization, prompts good crystallinity, conductivity and finally contributes towards improved storage performance. Thus the above prepared conducting polymer turned out to be a promising material for energy storage applications and further studies are going on to confirm its applicability in electrochemical supercapacitors.

Conflicts of interest

"There are no conflicts to declare".

Acknowledgements

The authors acknowledge Director and Principal, Rajagiri School of Engineering & Technology and Bharata Mata College for the

support of this work. Analytical support from Sophisticated Test and Instrumentation Centre, Cochin University of Science and Technology, School of Pure & Applied Physics, Mahatma Gandhi University and Department of Physics, Maharajas College, Ernakulam are also acknowledged.

References

[1] W. Chen, R.B. Rakhi, H.N. Alshareef, Morphology-dependent enhancement of the pseudocapacitance of template-guided tunable polyaniline nanostructures, J. Phys. Chem. C 117 (2013) 15009–15019, https://doi.org/10.1021/jp405300p.

[2] A. Khosrozadeh, M.A. Darabi, M. Xing, Q. Wang, Flexible electrode design: fabrication of freestanding polyaniline-based composite films for high-performance supercapacitors, ACS Appl. Mater. Interfaces 8 (2016) 11379–11389, https://doi.org/10.1021/acsami.5b11256.

[3] K. Pandey, P. Yadav, I. Mukhopadhyay, Elucidating the effect of copper as a redox additive and dopant on the performance of a PANI based supercapacitor, Phys. Chem. Chem. Phys. 17 (2015) 878–887, https://doi.org/10.1039/C4CP04321A.

[4] E. E, A. Sathiyan, R. S, J.S. E, P.M. J, Polyaniline based charcoal/Ni nanocomposite material for high performance supercapacitor, Sustain. Energy Fuels (2017), https://doi.org/10.1039/C7SE00490G.

[5] W. Fan, C. Zhang, W.W. Tjiu, K.P. Pramoda, C. He, T. Liu, Graphene-wrapped polyaniline hollow spheres as novel hybrid electrode materials for supercapacitor applications Graphene-wrapped polyaniline hollow spheres as novel hybrid electrode materials for supercapacitor applications, ACS Appl. Mater. Interfaces (2013), https://doi.org/10.1021/am4003827.

[6] J.W. Jeon, S.R. Kwon, F. Li, J.L. Lutkenhaus, Spray-on polyaniline/poly(acrylic acid) electrodes with enhanced electrochemical stability, ACS Appl. Mater. Interfaces 7 (2015) 24150–24158, https://doi.org/10.1021/acsami.5b07459.

[7] F.A. Rafiqi, K. Majid, Synthesis, characterization, luminescence and magnetic properties of composite of polyaniline with nickel bisacetylacetonate complex, Polym. Sci. Ser. B. 58 (2016) 371–383, https://doi.org/10.1134/S156009041603012X.

[8] W. Wang, S.P. Gumfekar, Q. Jiao, B. Zhao, Ferrite-grafted polyaniline nanofibers as electromagnetic shielding materials, J. Mater. Chem. C. 1 (2013) 2851, https://doi.org/10.1039/c3tc00757j.

[9] M.R. Sovizi, Z. Fahimi Hassan Gheshlaghi, Enhancement in electrochemical performances of Li–S batteries by electrodeposition of sulfur on polyaniline–dodecyl benzene sulfonic acid–sulfuric acid (PANI–DBSA–H_2SO_4) honeycomb structure film, New J. Chem. (2018), https://doi.org/10.1039/C7NJ05037B.

[10] Z. Wang, Q. Li, F. Besenbacher, M. Dong, Facile Synthesis of Single Crystal PtSe 2 Nanosheets for Nanoscale Electronics, 2016, pp. 1–6, https://doi.org/10.1002/adma.201602889.

[11] Z. Wang, Q. Li, M. Dong, H. Xu, C.D. Petersen, Q. Yang, D. Chengc, D. Caoc, F. Besenbachera, Jeppe V. Lauritsena, S. Helvegd, Controllable etching of MoS2 basal planes for enhanced hydrogen evolution through the formation of active edge sites, Nano Energy (2018), https://doi.org/10.1016/j.nanoen.2018.04.067.

[12] Z. Wang, Q. Li, Y. Chen, B. Cui, Y. Li, F. Besenbacher, M. Dong, The ambipolar transport behavior of WSe 2 transistors and its analogue circuits, NPG Asia Mater. (2018) 703–712, https://doi.org/10.1038/s41427-018-0062-1.

[13] W.A. Marmisollé, O. Azzaroni, Recent developments in the layer-by-layer assembly of polyaniline and carbon nanomaterials for energy storage and sensing applications. From synthetic aspects to structural and functional characterization, Nanoscale 8 (2016) 9890–9918, https://doi.org/10.1039/C5NR08326E.

[14] H. Wang, J. Lin, Z.X. Shen, Polyaniline (PANi) based electrode materials for energy storage and conversion, J. Sci. Adv. Mater. Dev. 1 (2016) 225–255, https://doi.org/10.1016/j.jsamd.2016.08.001.

[15] M. Kotal, A.K. Thakur, A.K. Bhowmick, Polyaniline-carbon nanofiber composite by a chemical grafting approach and its supercapacitor application, ACS Appl. Mater. Interfaces 5 (2013) 8374–8386, https://doi.org/10.1021/am4014049.

[16] X. Li, C. Zhang, S. Xin, Z. Yang, Y. Li, D. Zhang, P. Yao, Facile synthesis of MoS2/reduced graphene Oxide@Polyaniline for high-performance supercapacitors, ACS Appl. Mater. Interfaces 8 (2016) 21373–21380, https://doi.org/10.1021/acsami.6b06762.

[17] R. Ramkumar, M.M. Sundaram, Electrochemical synthesis of polyaniline cross-linked $NiMoO_4$ nanofibre dendrites for energy storage devices, New J. Chem. 40 (2016) 7456–7464, https://doi.org/10.1039/C6NJ00521G.

[18] P.K. Jha, B. Dhara, N. Ballav, Nanofibers to nanocuboids of polyaniline by lead nitrate: hierarchical self-assembly with lead ions, RSC Adv. (2014) 9851–9855, https://doi.org/10.1039/c3ra46691d.

[19] O.P. Dimitriev, Doping of polyaniline by transition metal salts: effect of metal cation on the film morphology, Synth. Met. 142 (2004) 299–303, https://doi.org/10.1016/j.synthmet.2003.10.003.

[20] T.D. Kose, Studies on transport properties of polyaniline transition metal salt composites, J. Compos. Mater. 45 (2011) 831–837, https://doi.org/10.1177/0021998310376114.

[21] O.P. Dimitriev, Doping of polyaniline by transition-metal salts, Macromolecules 37 (2004) 3388–3395.

[22] C. Yang, C. Chen, Synthesis, characterisation and properties of polyanilines containing transition metal ions, Synth. Met. 153 (2005) 133–136.

[23] A. Chiolerio, S. Bocchini, M. Crepaldi, K. Bejtka, Bridging electrochemical and electron devices : fast resistive switching based on polyaniline from one pot synthesis using FeCl 3 as oxidant and co-doping agent, Synth. Met. 229 (2017) 72–81, https://doi.org/10.1016/j.synthmet.2017.05.001.

[24] G.D. Nestorović, K.B. Jeremić, S.M. Jovanović, Kinetics of aniline polymerization initiated with iron(III) chloride, J. Serb. Chem. Soc. 71 (2006) 895–904, https://doi.org/10.2298/JSC0609895N.

[25] X.S. Du, C.F. Zhou, Y.W. Mai, Facile synthesis of Hierarchical polyaniline nanostructures with dendritic nanofibers as scaffolds, J. Phys. Chem. C 112 (2008) 19836–19840, https://doi.org/10.1021/jp8069404.

[26] Y. Hu, K. Masashi, T. Naoki, Polymerization of Aniline Using Iron(lll) Catalyst and Ozone and Kinetics of Oxidation Reactions in the Catalytic System, vol. 287, 2002, p. 503.

[27] J. Li, M. Cui, Y. Lai, Z. Zhang, H. Lu, J. Fang, Y. Liu, Investigation of polyaniline co-doped with Zn2+ and H+ as the electrode material for electrochemical supercapacitors, Synth. Met. 160 (2010) 1228–1233.

[28] D. Ghosh, S. Giri, A. Mandal, C.K. Das, Supercapacitor based on H+ and Ni2+ co-doped polyaniline–MWCNTs nanocomposite: synthesis and electrochemical characterization, RSC Adv. 3 (2013) 11676, https://doi.org/10.1039/c3ra40955d.

[29] P. Paik, R. Manda, C. Amgoth, K. Santhosh Kumar, Polyaniline nanotubes with rectangular-hollow-core and its self-assembled surface decoration: high conductivity and dielectric properties, RSC Adv. 4 (2014) 12342–12352, https://doi.org/10.1039/C3RA47155A.

[30] X.S. Du, C.F. Zhou, G.T. Wang, Y.W. Mai, Novel solid-state and template-free synthesis of branched polyaniline nanofibers, Chem. Mater. 20 (2008) 3806–3808, https://doi.org/10.1021/cm800689b.

[31] G. Ćirić-Marjanović, M. Trchová, J. Stejskal, MNDO-PM3 study of the early stages of the chemical oxidative polymerization of aniline, Collect. Czech Chem. Commun. 71 (10) (2006) 1407–1426.

[32] Z. Chuanqiang, H. Jie, S. Genping, G. Rong, Polyaniline hierarchical structures synthesized in aqueous solution: micromats of nanofibers, Macromolecules 40 (2007) 7075–7078, https://doi.org/10.1021/ma071400a.

[33] P. Asen, S. Shahrokhian, A.I. Zad, Transition metal ions-doped polyaniline/graphene oxide nanostructure as high performance electrode for supercapacitor applications, J. Solid State Electrochem. (2017) 1–14, https://doi.org/10.1007/s10008-017-3831-9.

[34] H. Xu, J. Wu, C. Li, J. Zhang, J. Liu, Investigation of polyaniline films doped with Fe3+ as the electrode material for electrochemical supercapacitors, Electrochim. Acta 165 (2015) 14–21, https://doi.org/10.1016/j.electacta.2015.01.224.

[35] A. Kellenberger, E. Dmitrieva, L. Dunsch, The stabilization of charged states at phenazine-like units in polyaniline under p-doping: an in situ ATR-FTIR spectroelectrochemical study, Phys. Chem. Chem. Phys. 13 (2011) 3411, https://doi.org/10.1039/c0cp01264e.

[36] P. Anilkumar, M. Jayakannan, New Renewable Resource Amphiphilic Molecular Design for Size-Controlled and Highly Ordered Polyaniline Nanofibers New Renewable Resource Amphiphilic Molecular Design for Size-Controlled and Highly Ordered Polyaniline Nanofibers, 2006, pp. 5952–5957, https://doi.org/10.1021/la060173n.

[37] O. Abdulrazzaq, S.E. Bourdo, V. Saini, F. Watanabe, B. Barnes, A. Ghosh, A.S. Biris, Tuning the work function of polyaniline via camphorsulfonic acid: an X-ray photoelectron spectroscopy investigation, RSC Adv. 5 (1) (2015) 33–40.

[38] A. Kumar, A. Saxena, A. De, R. Shankar, S. Mozumdar, Facile synthesis of size tunable copper and copper oxide nanoparticles using reverse microemulsion, RSC Adv. (2013).

[39] M.N. Nadagouda, R.S. Varma, Green approach to bulk and template-free synthesis of thermally stable reduced polyaniline nanofibers for capacitor applications, Green Chem. 9 (2007) 632, https://doi.org/10.1039/b614633c.

[40] J. Zhu, H. Gu, Z. Luo, N. Haldolaarachige, D.P. Young, S. Wei, Z. Guo, Carbon nanostructure-derived polyaniline metacomposites: electrical, dielectric, and giant magnetoresistive properties, Langmuir 28 (2012) 10246–10255, https://doi.org/10.1021/la302031f.

[41] H. Xu, J. Wu, C. Li, J. Zhang, J. Liu, Investigation of polyaniline films doped with Fe3+ as the electrode material for electrochemical supercapacitors, Electrochim. Acta 165 (2015) 14–21, https://doi.org/10.1016/j.electacta.2015.01.224.

[42] V.P. Anju, S.K. Narayanankutty, Polyaniline coated cellulose fiber/polyvinyl alcohol composites with high dielectric permittivity and low percolation threshold, AIP Adv. 6 (2016), https://doi.org/10.1063/1.4940664.

[43] M. Niranjana, L. Yesappa, S.P. Ashokkumar, H. Vijeth, S. Raghu, H. Devendrappa, Localized polarons in in situ synthesized polyaniline nanocomposite improve the morphology and the thermal and electrical conductivity, RSC Adv. 6 (2016) 115074–115084, https://doi.org/10.1039/C6RA24137A.

[44] M. Wan, A.K. Srivastava, P.K. Dhawan, R.R. Yadav, S.B. Sant, R. Kripal, J.-H. Lee, High dielectric response of 2D-polyaniline nanoflake based epoxy nanocomposites, RSC Adv. 5 (2015) 48421–48425, https://doi.org/10.1039/C5RA05660H.

[45] J. Tahalyani, K.K. Rahangdale, R. Aepuru, B. Kandasubramanian, S. Datar, Dielectric investigation of a conducting fibrous nonwoven porous mat fabricated by a one-step facile electrospinning process, RSC Adv. 6 (2016) 36588–36598, https://doi.org/10.1039/C5RA23012H.

[46] M.D.A. Khan, A. Akhtar, S.A. Nabi, Investigation of the electrical conductivity

and optical property of polyaniline-based nanocomposite and its application as an ethanol vapor sensor, New J. Chem. 39 (2015) 3728–3735, https://doi.org/10.1039/C4NJ02260B.
[47] X. Zhang, Q. He, H. Gu, S. Wei, Z. Guo, Polyaniline stabilized barium titanate nanoparticles reinforced epoxy nanocomposites with high dielectric permittivity and reduced flammability, J. Mater. Chem. C. 1 (2013) 2886, https://doi.org/10.1039/c3tc30129j.
[48] D.S. Patil, J.S. Shaikh, S.A. Pawar, R.S. Devan, Y.R. Ma, A.V. Moholkar, J.H. Kim, R.S. Kalubarme, C.J. Park, P.S. Patil, Investigations on silver/polyaniline electrodes for electrochemical supercapacitors, Phys. Chem. Chem. Phys. 14 (2012) 11886, https://doi.org/10.1039/c2cp41757j.
[49] F.A. Rafiqi, K. Majid, Synthesis, characterization, luminescence and magnetic properties of composite of polyaniline with nickel bisacetylacetonate complex, Polym. Sci. Ser. B. 58 (2016) 371–383, https://doi.org/10.1134/S156009041603012X.
[50] S.B. Kulkarni, U.M. Patil, I. Shackery, J.S. Sohn, S. Lee, B. Park, S. Jun, High-performance supercapacitor electrode based on a polyaniline nanofibers/3D graphene framework as an efficient charge transporter, J. Mater. Chem. 2 (14) (2014) 4989–4998.
[51] W. Chen, R.B. Rakhi, H.N. Alshareef, Morphology-dependent enhancement of the pseudocapacitance of template-guided tunable polyaniline nanostructures, J. Phys. Chem. C 117 (2013) 15009–15019, https://doi.org/10.1021/jp405300p.
[52] V. Kumar, P.S. Lee, Redox active polyaniline-h-MoO_3 hollow nanorods for improved pseudocapacitive performance, J. Phys. Chem. C 119 (2015) 9041–9049, https://doi.org/10.1021/acs.jpcc.5b00153.
[53] W. Zhang, Y. Zhou, K. Feng, J. Trinidad, A. Yu, B. Zhao, Morphologically controlled bioinspired Dopamine-polypyrrole nanostructures with tunable electrical properties, Adv. Electron. Mater. 1 (2015) 1–10, https://doi.org/10.1002/aelm.201500205.
[54] B. Liang, Z. Qin, J. Zhao, Y. Zhang, Z. Zhou, Y. Lu, Controlled synthesis, core–shell structures and electrochemical properties of polyaniline/polypyrrole composite nanofibers, J. Mater. Chem. A. 2 (2014) 2129–2135, https://doi.org/10.1039/C3TA14460G.
[55] S. Yu, D. Liu, S. Zhao, B. Bao, C. Jin, W. Huang, H. Chen, Z. Shen, Synthesis of wood derived nitrogen-doped porous carbon–polyaniline composites for supercapacitor electrode materials, RSC Adv. 5 (2015) 30943–30949, https://doi.org/10.1039/C5RA01949D.
[56] Y. Luo, W. Hong, Z. Xiao, H. Bai, A high-performance electrochemical supercapacitor based on a polyaniline/reduced graphene oxide electrode and a copper (ii) ion active electrolyte, Pubs.Rsc.Org. (2017), https://doi.org/10.1039/C7CP07156F. P.C.C. Physics, undefined 2018.
[57] W.A. Marmisollé, M.I. Florit, D. Posadas, A formal representation of the anodic voltammetric response of polyaniline, J. Electroanal. Chem. 655 (2011) 17–22, https://doi.org/10.1016/j.jelechem.2011.02.019.
[58] A.N. Golikand, M. Bagherzadeh, Z. Shirazi, Evaluation of the polyaniline based nanocomposite modified with graphene nanosheet , carbon nanotube , and Pt nanoparticle as a material for supercapacitor, Electrochim. Acta (2017), https://doi.org/10.1016/j.electacta.2017.07.011.
[59] T. Li, Z. Qin, B. Liang, F. Tian, J. Zhao, N. Liu, M. Zhu, Morphology-dependent capacitive properties of three nanostructured polyanilines through interfacial polymerization in various acidic media, Electrochim. Acta 177 (2015) 343–351, https://doi.org/10.1016/j.electacta.2015.03.169.
[60] M.R. Sovizi, M.R. Yaftian, S.T. Seyyedin, A reduced graphene oxide@sulfur nanocomposite as a high-capacity host matrix for advanced lithium–sulfur batteries, New J. Chem. (2017), https://doi.org/10.1039/C7NJ00123A.
[61] Q. Wang, Q. Zong, C. Zhang, H. Yang, Q. Zhang, Network structure of SnO_2 hollow sphere/PANI nanocomposites for electrochemical performance, Dalt. Trans. (2018), https://doi.org/10.1039/C8DT00056E.